International Journal of Engineering Trends and Technology
ISSN: 2231 – 5381 /doi:10.14445/22315381/IJETT-V70I2P218
Volume 70 Issue 2, 151-162, February, 2022

Original Article

DBR Laser Design Using Vanadium Doped Silicon-carbide Active Region to Achieve Wide Tuning Range for Telecommunications Application in the 1300nm Window

Patrick Mumba [1], Franklin Manene[2], Stephen Musyoki[3]

[1]*Department of Electrical Engineering, Pan African Univ. Inst. of Basic Sciences Technology and Innovation, Nairobi, Kenya.*

[2]*Egerton university. Kenya.*

[3]*School of Electrical and Electronics Engineering, Technical Univ. of Kenya, Nairobi, Kenya*

mumba.patrick@students.jkuat.ac.ke[1], manenef@gmail.com[2], smusyoki@yahoo.com[3]

Abstract *- The 5G technology is expected to use tunable lasers for wavelength selection during optical signal transmission. To accommodate the growing data demand, there is a need to develop lasers with a larger tuning range. In most lasers, Indium gallium arsenide phosphide (InGaAsP), Aluminum Gallium Arsenide (AlGaAs), and Gallium Arsenide (GaAs) have been used for the gain medium due to their direct bandgap and strong optical transitions. However, they have limitations such as low SMSR, low output power due to their narrow bandgap, and a narrow tuning range below 20nm. In this paper, vanadium-doped silicon-carbide was used in the active section of the Distributed Bragg Reflector (DBR) laser to achieve a wide tuning range, high SMSR, low threshold current, and high output power at a low gain current. The fundamental advantages of vanadium-doped silicon-carbide, including fast optical transitions, make its operation in the O-band (1278-1388 nm) possible. The DBR laser architecture design was adopted and designed in Ansys Lumerical. This work established that the use of Vanadium doped silicon-carbide in the active region provides a tuning range of at least 22nm wavelength, a threshold current was found to be 22.5mA with an optical output power of 13mW at the gain current of 120mA, and side mode suppression ratio (SMSR) of at least 45dB.*

Keywords — *Distributed Bragg Reflector laser, Vanadium-doped silicon carbide.*

I. INTRODUCTION

The demand for high data rates has prompted the need for wide deployment of fifth-generation (5G) communication technology with a peak data rate of 20Gbs [1], the latency of less than 1ms, 1000x bandwidth per unit area, 10-100x number of connected devices, perception of 99.9% availability, perception of 100% coverage, 90% reduction in network energy usage, up to ten-year battery life for low power machine type devices [2][3]. 5G is set to implement Radio over fibre (5G-RoF) technologies which combine the advantages of wireless networks over fibre technologies by transmitting a radio signal on a fibre transmission line. RoF advantages include bandwidth larger than that of Radiofrequency technology, facile in maintenance and implementation, and minimum loss due to attenuation [4]. Unlike the 4G technologies, which used the orthogonal frequency division multiplexing (OFDM) technique, 5G will employ the hybrid Time/Wavelength Division Multiplexing (TWDM) technique for serving higher user density Radio over Fibre (RoF) antenna sites on the optical network infrastructure [5]. The TWDM passive optical network (PON) architecture is implemented with tunable lasers to meet the demand for high data rates and have low latency. In a traditional Optical network unit, several tunable lasers have been suggested, such as an embedded tunable laser [6], III-V elements based on silicon tunable lasers [7], Indium phosphate (InP) based on silicon tunable lasers [8], and many more. However, there is still room for improvement in the tuning range to surpass the recently developed ranges (which include 12.12nm [9], 14nm [10], 20nm [11], 8nm [12], etc.) to cover a wider range of the spectrum and achieve high data transmission. The design of a laser depends on many factors, including the radiating material in its active region and the dimensions of the active region.

Many semiconductor elements such as Indium Gallium Arsenide phosphate (InGaAsP), Gallium Arsenide (GaAs), Aluminium Gallium Arsenide (AlGaAs), etc. have been used as light-emitting materials in Light Emitting Diodes (LEDs) and Lasers because of their direct bandgap structure and strong optical transitions [13]. Lasers with quantum wells in the active region tend to show an increase in the threshold current and a significant decrease in efficiency with temperature variation [14]. This threshold current increase with temperature in Quantum Well lasers is due to higher threshold density and decrease of the gain at high temperatures.

Other limitations include low output power, narrow tuning range to meet the increasing demand for high data rates in the TWDM Passive Optical Network for 5G [9], low side mode suppression ratio (SMSR) of about 35dB

[15] (this implies that most of the transmission power is shared with side modes rendering the transmission power in the main mode low). Due to these limitations, other semiconductor materials have been studied to find a stable material with better features. In most studies, wide-bandgap semiconductors have picked the interest of researchers because of their long tangible spin and spin-photon coupling through bright optical transitions that can be manipulated into working in a Quantum-Well structure [16][17]. Their indirect-band gap is the challenge faced; this is rectified by doping impurities in a semiconductor to match its lattice to emit directly in a telecommunication wavelength window. The compound silicon-carbide (SiC) is one of the most studied semiconductor materials. It has been illustrated that diamond and SiC are capable of having many spin-active color centers that could be suitable properties in the semiconductor industry [18]. SiC advantages include functioning in environments where high frequency, high temperature, and high power are needed [19]. Experiments have been carried out to prove that silicon-carbide can emit light in an 830nm telecommunication window [14] and 1300nm telecommunication window when doped with impurities to match its lattice [20][16][21]. When doped with appropriate impurities, hexagonal silicon-carbide (6H-SiC and 4H-SiC) can radiate in the 830nm telecommunications window. Studies have been carried out on the transition-metal impurity defects in SiC. The element Chromium Cr^{4+} was found to have spins in SiC that can be manipulated to resonate with the first state of excitation of Zero Phonon Line (ZPL) optical transition [17][18][22]. Molybdenum impurities have shown ZPL transitions at 1121nm and 1076nm in 6H-SiC and 4H-SiC, respectively, and it also forms deep level-defects in stable charge states, each with a unique value for its spin and optical transitions in the near-infrared region [21][23].

Vanadium (V) impurities in SiC form colour centre emission in telecommunication wavelength regime meeting the generation of large photon states required in the telecommunications wavelength regime [14][16]. Furthermore, V centres in SiC create the prospect of a single-photon emitting diode electrically driven in the host, which is the most preferred material in the semiconductor industry [20]. Vanadium impurities have shown ZPL transitions around 1300nm [21][16]. G. Wolfowicz et al. created isolated near-surface dopants of vanadium in silicon-carbide. Their results showed optical emission wavelengths in 4H-SiC 1278.808nm and 1335.331nm with radiative recombination lifetimes of 167ns and 45ns, respectively [24].

L.Spindlberger et al. [25] presented the optical properties of 4H-SiC with tetravalent Vanadium impurities with the aim of applications in telecommunications and quantum information. Their investigation of V impurities in SiC showed narrow optical emission lines in the telecommunications window at 1334 nm wavelength, to be exact, with an optical lifetime of 43 ns. The time and temperature-dependent measurements permitted them to clarify unassigned spectrum features and other attractive features, including a narrow inhomogeneous line-width and rapid optical transitions [25].

The optical properties of V dopant in SiC, such as 1300 nm emission wavelength and the fact that SiC has a high output power [26], allow us to suggest it as an active layer material in the Distributed Bragg Reflector (DBR) laser design to operate in the telecommunication transmission windows. The parameters and the optical constants, including refractive index and energy bandgap, are not given in the literature review. In this work, formulations and calculations were done to obtain the optical constants used to present a tunable DBR laser with silicon-carbide doped with impurities of Vanadium (V) in the active region to achieve a wide tuning range and a higher side mode suppressing ratio (SMSR). To the best of our knowledge, the usage of vanadium doped silicon-carbide in the active region of a DBR laser has not been done before.

The rest of this work is arranged as follows, the experimental setup and methodology are presented in section 2, section 3 discusses results, and section 4 presents the conclusion drawn. Ansys Lumerical software was used for simulations.

II. EXPERIMENTAL SETUP

The DBR laser was designed with three sections, as shown in figure **1**. The lasing frequency is in the 1300 nm telecommunication window in this work.

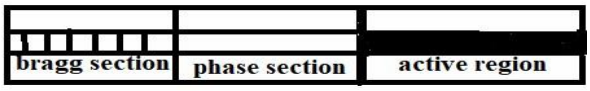

Fig. 1 DBR laser schematic

The Bragg frequency was set to the required lasing frequency $f_0 = 224.732\,THz$ or $\lambda_0 = 1334nm$ to allow feedback at this frequency. To ensure a single dominant resonance occurring at the Bragg frequency, the optical cavity length is set such that one of the Fabry-Perot modes should be supported with only the reflectance situated at the facet and not on the Bragg section. A phase section was added to the design for tuning. In this research, the active section was designed and analyzed first, followed by the phase and Bragg sections which were added to adapt the Bragg section's effective refractive index to that of the Active section.

A. Active Region Design

It is not possible to use Vanadium to achieve doping of SiC in Ansys Lumerical interconnect module. However, the required optical constants were obtained from relevant literature. In this work, data was collected from the literature discussed below and applied to obtain the required optical constants before the design of the active region circuit shown in figure **2**.

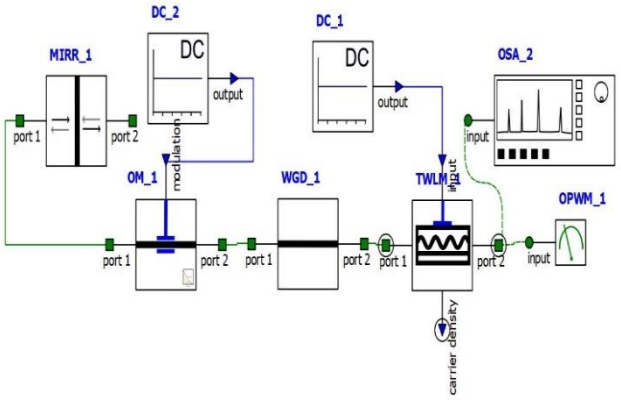

Fig. 2 Fabry-Perot Circuit

The active region circuit in figure **2** is viewed as a Fabry-Perot laser where MIRR_1 represents the mirror facet to reflect light back into the resonating cavity, OM_1 is a modulator, and WGD_1 is a waveguide together they form a phase section used for smooth transitioning from one wavelength to another. TWLM_1 is a Traveling Wave Laser Model representing the Active region (Gain medium) where stimulated emission occurs. On port 2 of the TWLM_1, partial reflectivity is configured to reflect some photons back into the resonating cavity, and some photons are emitted. On port 2, the optical spectrum analyzer (OSA_1) is attached to detect the optical spectrum, the optical power meter labelled OPWM_1 is used to study the threshold current and the output power of the Fabry-Perot laser. The Direct Current source labelled DC_1 is used to initiate radiation in the gain medium to have stimulated emission. DC_2 is used in tuning. In the Fabry-Perot circuit, DC_2 is set to zero. Therefore, the modulator acts as a waveguide.

a) Cavity length design

To ensure constructive interference, equation (1) was used to obtain the cavity length [27]:

$$N\lambda_0 = 2L \tag{1}$$

Where N is an integer, λ_0 is the lasing wavelength, and L is the cavity length. The lasing condition is given by the Round Trip (RT) amplification of a photon as given in equation (2), and this is used in obtaining net gain per unity length g (gain threshold parameter). [28]:

$$RT = e^{2Lg}(R_1R_2) = 1 \tag{2}$$

R_1 and R_2 represent the reflectivity of the facet mirrors of the optical cavity. Using equation (2), the expression for net gain threshold parameter of the cavity was obtained as shown in equation (3) [28]:

$$g = \frac{1}{2L} ln(\frac{1}{R1R2}) \tag{3}$$

The standard cavity length of a Fabry-Perot in fibres is in the range of 150µm – 1000µm [29]. In this work, the largest value possible was chosen for the active region design by setting the length of the active region to 999.3448µm using equation (1). The modulator labelled OM_1, and the waveguide labelled WGD_1 in figure 2 each has a length of 74.948µm which is a default value assigned by the Ansys Lumerical software [30]. Therefore, the total cavity (L) length obtained was L = 1149.241 µm. This length satisfies equation (1), with N = 1723, The reflectivity R_1 of the mirror labelled MIRR_1 in figure 2, and R_2 defined on port 2 of the TWLM_1 circuit in figure 2 are 0.999 and 0.7 respectively. Using equation (3), the gain threshold parameter was found to be:

$$g = \frac{1}{2\,x\,1149.241\,x10^{-6}} \ln\left(\frac{1}{0.999X0.7}\right) = 155.61/m$$

The gain result was used to calculate the Gain coefficient used in the design of the Fabry-Perot laser. The gain coefficient defines the change in photons' density as they move along the cavity length. The initial carrier density n_i was set to the default setting for TWLM in Ansys Lumerical, which is expressed in equation (4):

$$n_i = 1.5 \text{ x } 10^{24}\text{m}^{-3} \tag{4}$$

Equation (5) was used to calculate the gain coefficient a_p [31]:

$$a_p = \frac{g}{n_i} = \frac{155.61}{1.5\text{x}10^{24}} = 1.037\text{x}10^{-22}\text{m}^2 \tag{5}$$

b) Bandgap Energy of Vanadium Doped Silicon-Carbide

Given that the laser is to operate at the wavelength of 1334nm, the required bandgap energy is calculated using equation (6):

$$E_{.g.} = h\nu = \frac{hc}{\lambda} \tag{6}$$

$$E_{.g.} = \frac{hc}{\lambda_0} = \frac{6.62\text{x}10^{-34}\text{x } 3.0 \text{ x } 10^{8}}{1334\text{x}10^{-9}} = 1.4888 \text{ x } 10^{-19} joules$$

Where h = 6.62x10^{-34}J/Hz is plank's constant, c = 3.0 x 10^{8}m/s is light's speed, λ_0 = 1334nm wavelength of emission and v is light emission frequency. When expressed in electron volts, the above-calculated bandgap energy is 0.93 eV. The total bandgap energy of SiC is 3.2 eV. When doped with the neutral V^{4+} impurities, the ground state is raised by 1.6eV above the valence band of the polytypes 4H-SiC and 6H-SiC [24]. V^{+4} reduces the excited state energy of 4H-SiC from the 3.2eV by 0.6eV to 0.8eV [32]. Based on these findings, the calculations in this paper were done with an assumption that SiC was doped by V enough to reduce the excited state energy by 0.67eV. This is illustrated in figure **3**.

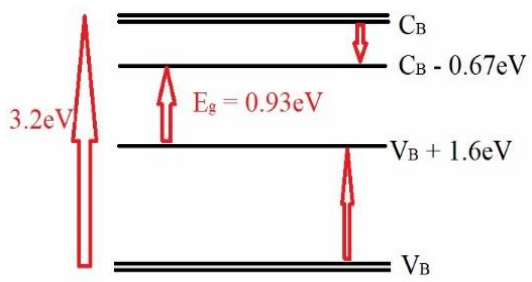

Fig. 3 Energy band gap of V doped SiC

This implies that the effective energy bandgap when both acceptors and donors doping are complete is 0.93 eV. From equation (6), this energy bandgap (E_g = 0.93) radiates at 1334nm wavelength.

c) Refractive index of V doped SiC

The refractive index was calculated using the Moss' relation as defined in equation (7) [33]:

$$n^4 E_g = 95\text{eV} \quad (7)$$

where: n is refractive index and E_g is energy bandgap. Therefore, refractive index is given as:

$$n = \sqrt[4]{(95\text{eV}/E_g)} = \sqrt[4]{(95\text{eV}/0.93\text{eV})} = 3.179$$

d) Radiative recombination coefficient

The optical properties of 4H-SiC with V^{4+} impurities give two radiative recombination lifetimes. In [25], fluorescence was spectrally resolved using blue excitation of defects, two emission wavelengths were observed. One was emitting at 1334nm wavelength with a radiative recombination lifetime of 43ns, and the other was emitting in the range of 1277.0 nm to 1280 nm [25]. In this work, the studied wavelengths were in the 1300nm telecommunication window; therefore, the 1334nm emission was studied. The radiative recombination rate was calculated using equation (8) [34]:

$$R_r = \frac{n_i}{\tau_r} = \frac{1.5\text{x}10^{24} m^{-3}}{43\text{x}10^{-9} s} = 3.488\text{x}10^{31} m^{-3}/s \quad (8)$$

Where n_i is the initial carrier density from equation (4), and τ_r is the radiative recombination lifetime. With an assumption that the non-radiative recombination and Auger recombination coefficients are negligible, the radiative recombination coefficient B is given by equation (9)[35]:

$$B = \frac{R_r}{n_i} = \frac{1}{\tau_r} = \frac{3.488\text{x}10^{31}\text{m}^{-3}/\text{s}}{1.5\text{x}10^{24} m^{-3}} = 0.2325x10^8/s \quad (9)$$

Based on the works done in [36], the typical value of the spontaneous emission factor (σ) is estimated to be $\sigma = 10^{-3}$.

The phase section and the gain section were implemented using the optical constants calculated above, and they are listed in Table 1. The Ansys Lumerical default values 5μm and 0.1μm for active region width and thickness respectively were adopted.

Table 1. List of Parameters for Active Region Design

Name	value
Radiative recombination constant	2.326 x 10^8/s
Spontaneous emission factor	10^{-3}
Initial carrier density	1.5 x 10^{23}m^{-3}
Centre frequency, wavelength	224.732 THz, 1334nm
Energy bandgap	0.93eV
Refractive index	3.179
Gain coefficient	1.0338 x 10^{-22} m^2
Active region width	5 μm
Left Mirror reflectivity	0.999
Right mirror reflectivity	0.7
Modulator frequency and length	224.732THz, 74.948μm
Waveguide frequency and length	224.732THz, 74.948μm
Active region thickness	0.1 μm

B. Bragg section design

The Ansys Lumerical default settings for the Bragg section were adopted. Changes were made to the waveguide Bragg grating default settings as follows; Bragg frequency was changed from 1550nm to 1334nm wavelength, the effective refractive index was changed from 1.447 to 3.179, adapting to the active region refractive index. Figure **4** shows the Bragg section circuit designed using the list of parameters shown in table 2 below.

Table 2. Bragg section constants

Name	value
Length	0.005m
Input parameter	Bragg frequency
Effective index	3.179
Bragg frequency	1334nm
Effective index change	0.0009 ac

Figure 4 illustrates the Bragg section implemented in Ansys Lumerical.

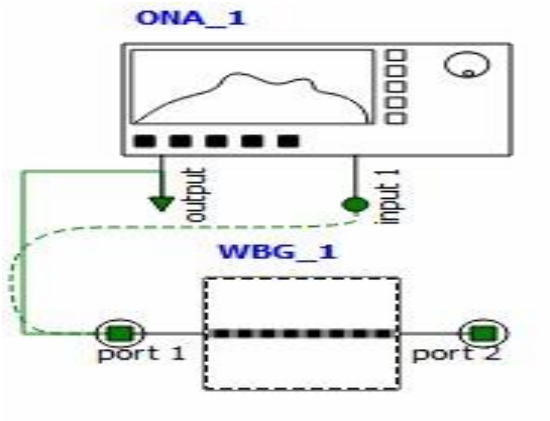

Fig. 4 Bragg section Circuit

The optical network analyzer (ONA) is used to view the Waveguide Bragg-Grating (WBG) reflectance curve. The Bragg section parameters in table 2 were used in the design, and the simulation was run in Ansys Lumerical. The results are discussed in the next section of this paper.

A full DBR laser with the calculated optical constants was implemented. The circuit is illustrated in figure **5**. The Terminal mirror shortened as MIRR_1 in figure **2** circuit was replaced by a Bragg section circuit from figure **4**, abbreviated as WBG_3 in figure **5**. Bragg lasing frequency was set at 224.732THz (1334nm wavelength).

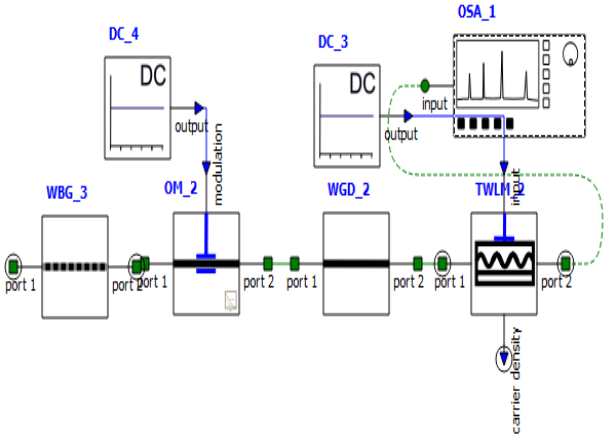

Fig. 5 V-doped SiC DBR laser

III. RESULTS AND DISCUSSION

A. Tuning Range

The Fabry-Perot circuit in figure **2** was implemented and simulated using the parameters in table 1. The results in figure **6** illustrate the corresponding spectrum as a result of the new material (V doped SiC) used in the active region:

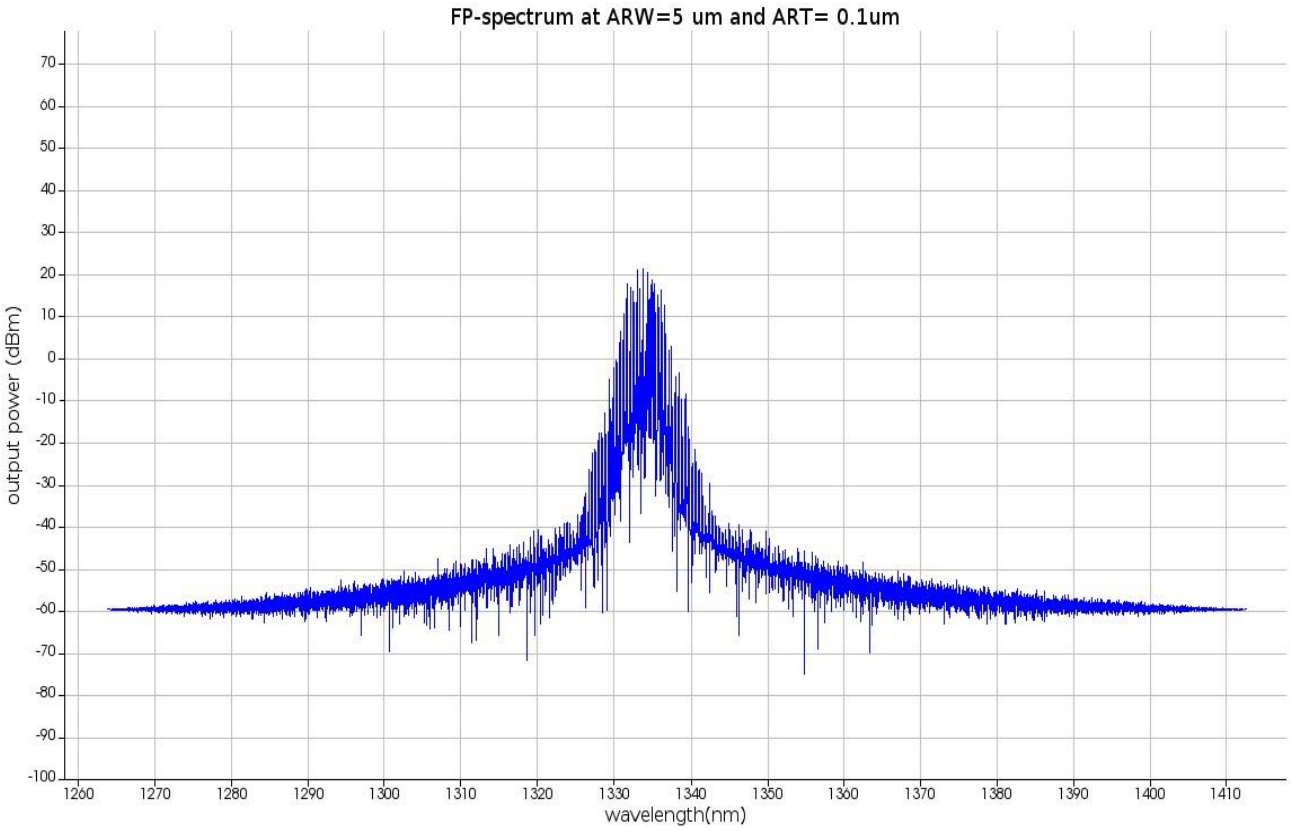

Fig. 6 (A)

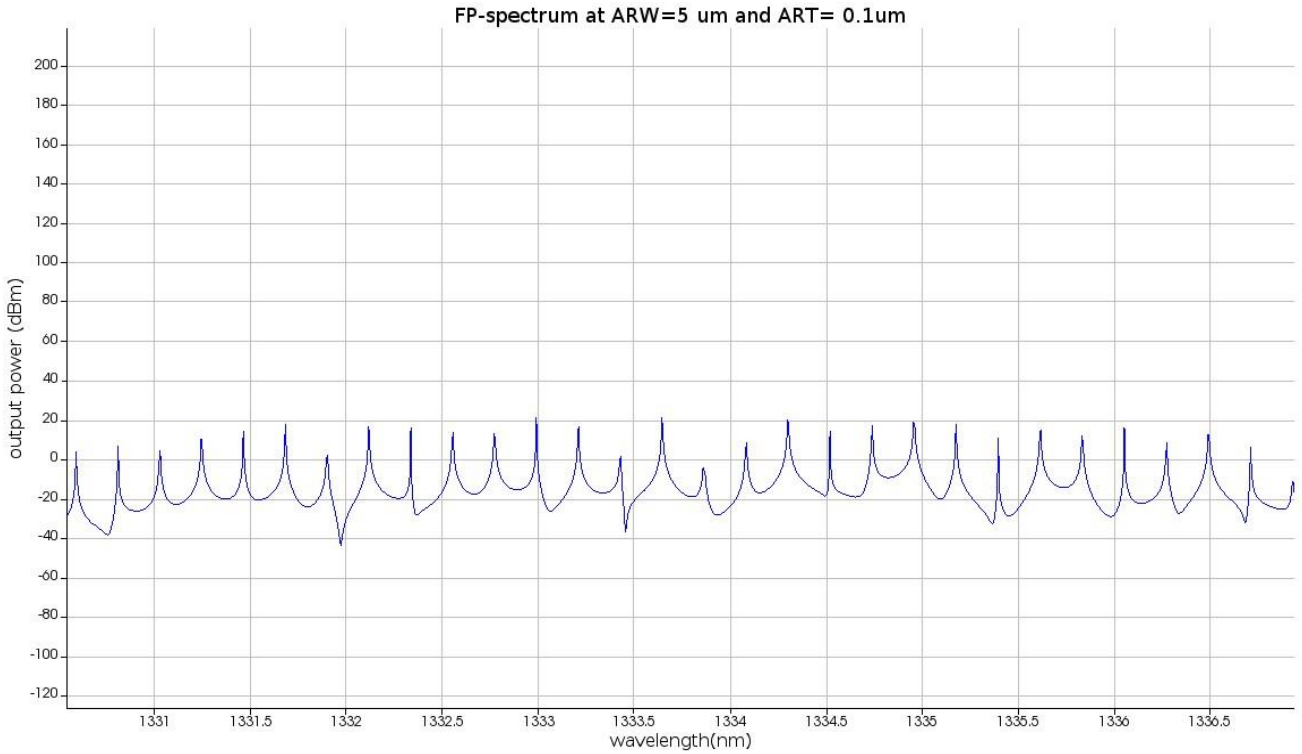

Fig. 6 (B)

Fig. 6: Fabry-Perot Spectrum with active region width set to 5µm and active region thickness set to 0.1µm.

The resulting spectrum was covering a narrow width at Full Width at Half Maximum (FWHM), and it was observed from the zoomed spectrum in figure **6**(B) that the signal impulses had noise in between. These cause interference during transmission. The active region thickness was reduced from 0.1um to 0.08um, and the active region width was reduced from 5um to 4um. The corresponding spectrum is illustrated in figure **7**:

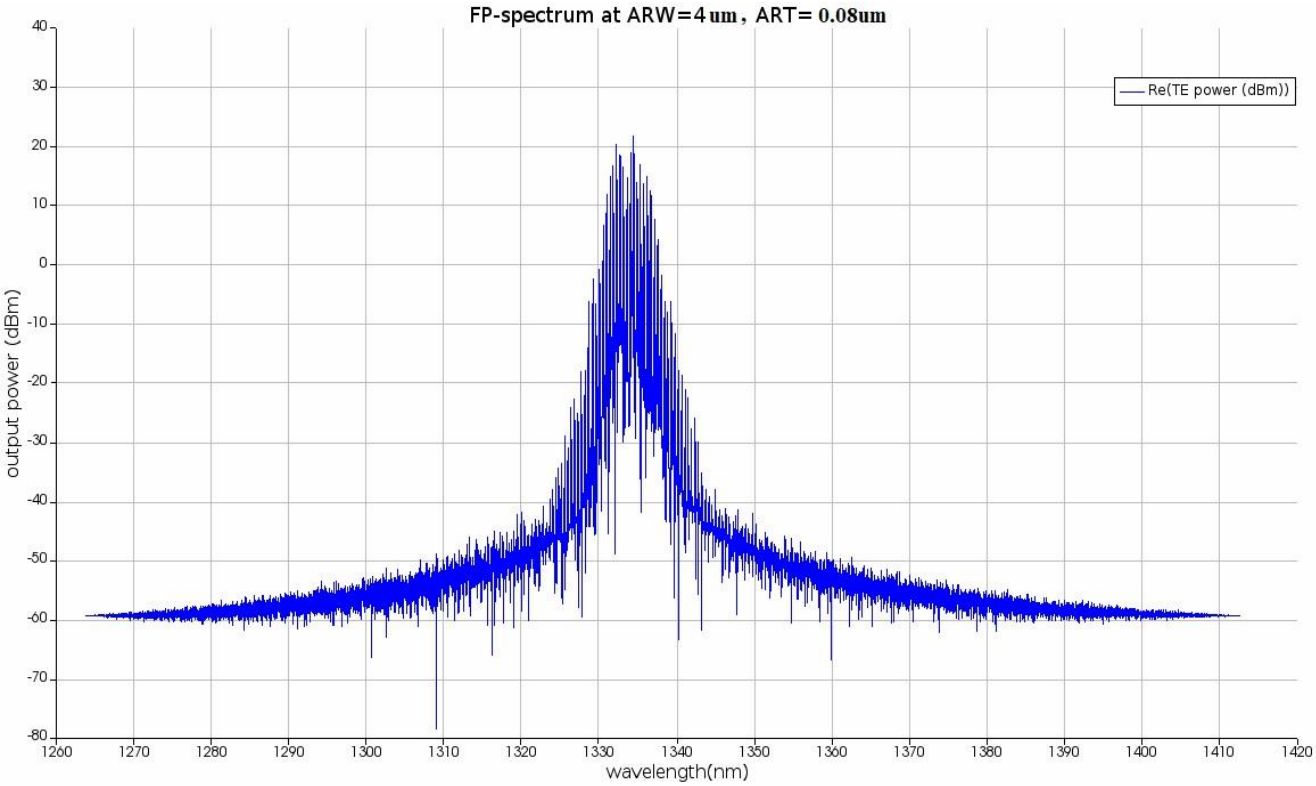

Fig. 7 (A)

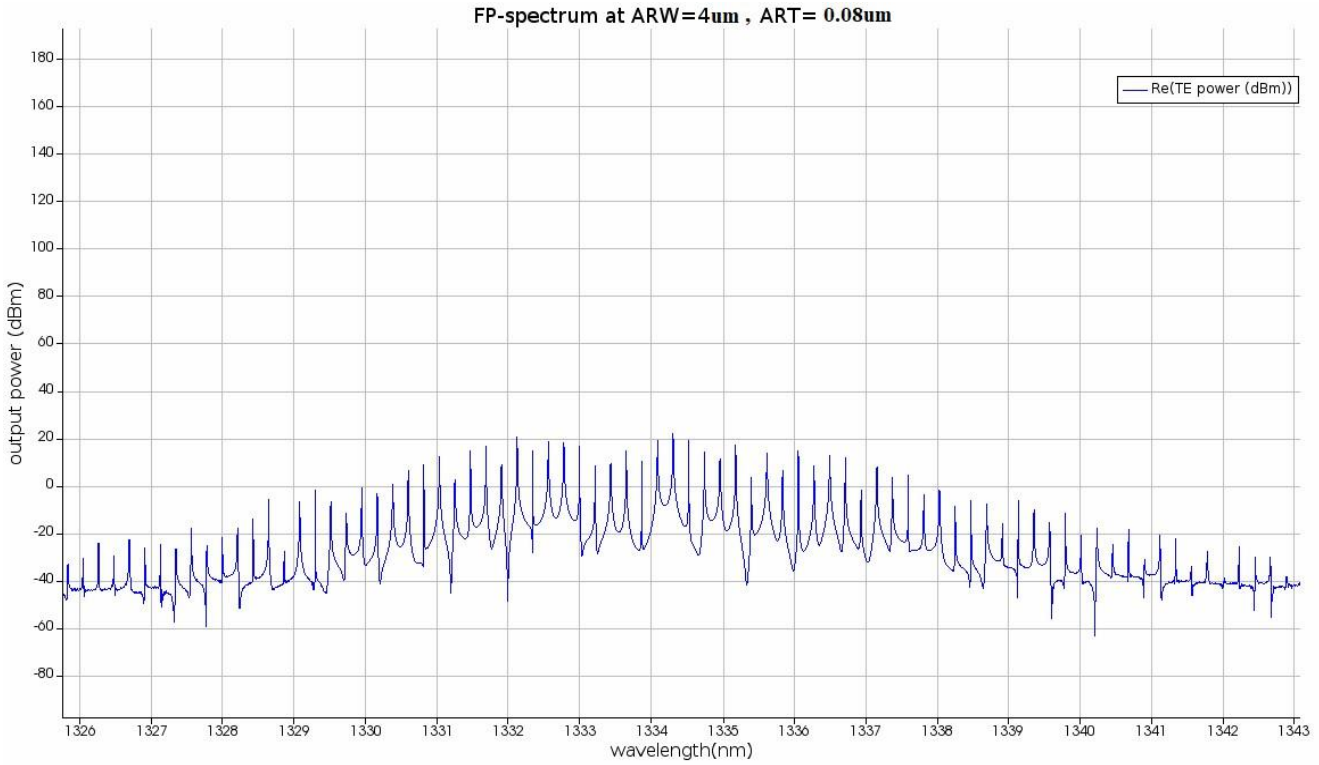

Fig. 7 (B)

Fig. 7: Fabry-Perot Spectrum with active region width set to 4μm and active region thickness set to 0.08μm.

It was observed that the reduction of the active region width and active region thickness led to the reduction in the number of noise impulses and also led to the increase in the spectral width coverage at FWHM. A better spectrum with less noise, more transmittable signal impulses and wide spectral coverage is obtained when the active region width was reduced to 2um, and the active region thickness was reduced to 0.01um. The resulting spectrum is shown in figure **8(A, B, C)** below. The tuning range width was determined from the spectral width covered at FWHM.

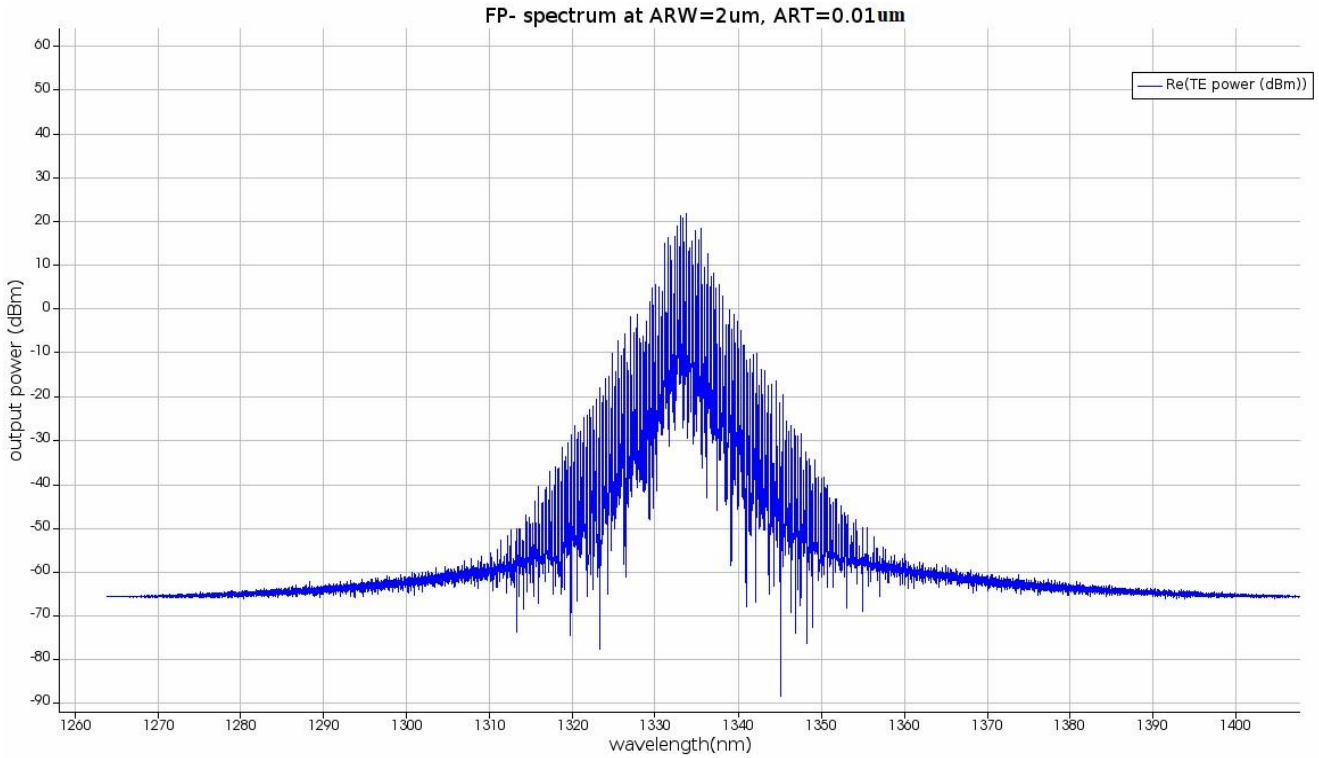

Fig. 8(A)

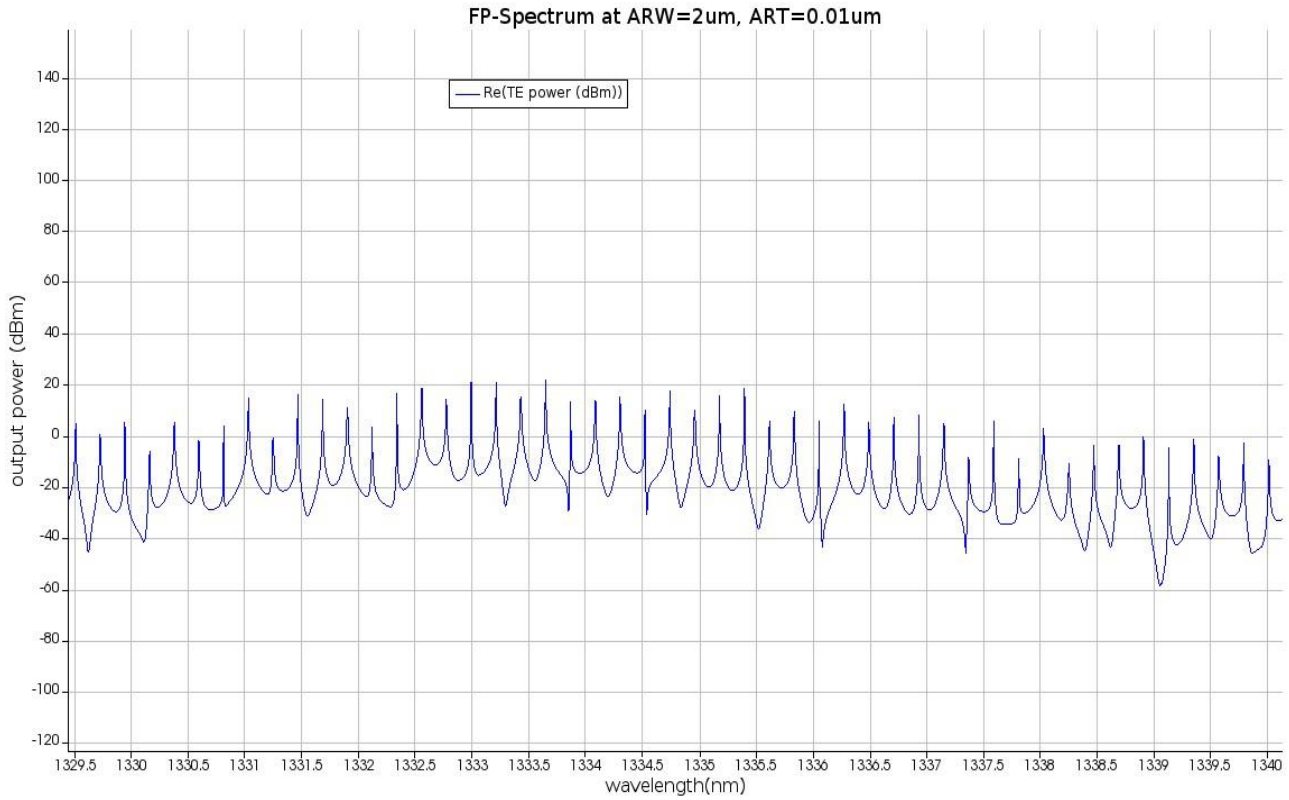

Fig. 8(B)

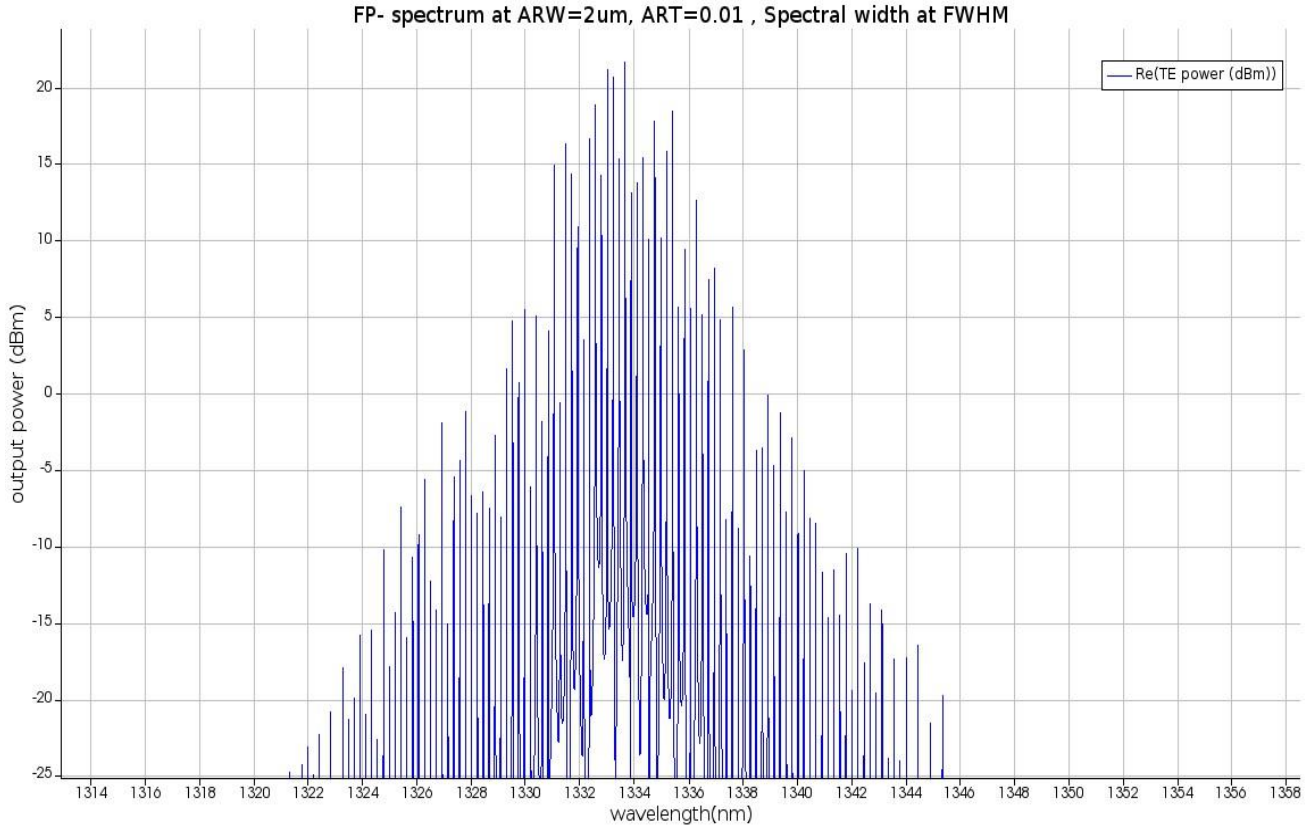

Fig. 8(C)

Fig. 8: Fabry-Perot spectral coverage at FHWM, Active Region Width (ARW) was set to 2 µm, and Active Region Thickness (ART) was set to 0.01 µm

Figure **8**(A) shows the corresponding spectrum at 2 µm active region width and 0.01 µm active region thickness, and its zoomed spectrum is in figure **8**(B), illustrating less noise in between signal impulses, it was observed from the Fabry-Perot spectrum in figure **8**(C), that the tuning range of at least 22nm was achieved at FWHM. The tuning range obtained in this work is larger than the tuning range of 8nm used in [12] by Y. Zhu et al. with the intent to send data using a 3s-DBR laser. It is also wider than the tuning range found by L. Han et al. [11], who had the tuning range of 20nm with InGaAsP in the active region, and it is also wider than the tuning range in a DBR laser designed by D. Zhou et al. [10] who established a tuning range of 14nm with InGaAlAs in the active region, it is also better than the tuning range by D. Zhou et al. [9] who had the tuning range of 12.12nm with InGaAlAs/InGaAsP DBR laser. Therefore, the usage of V doped SiC in the gain section has widened the tuning range of the DBR laser.

B. Threshold Current and Output Power

The threshold current (I_{th}) was measured through the optical power wavemeter (OPWM) shown in figure **2,** which gave the L-I curve in figure 9.

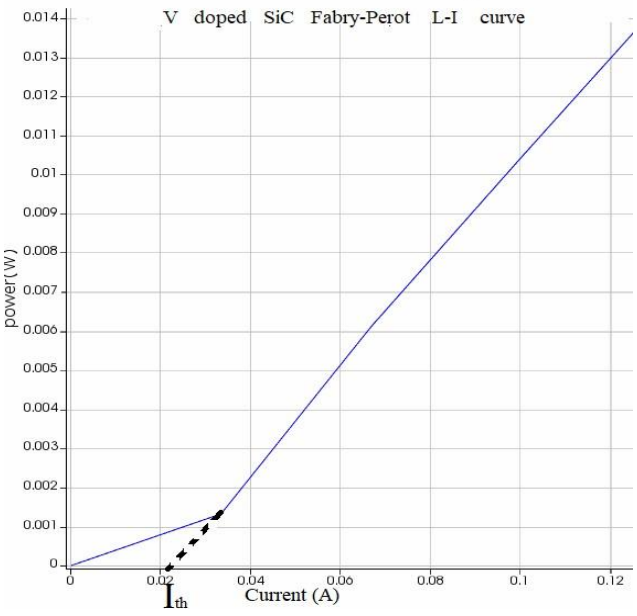

Fig. 9 Fabry-Perot L-I curve

The threshold current is found by calculating the gradient of the lasing curve, which is m = 0.1333, then setting the optical power to 0 and solving for the current, the threshold current is found to be $I_{th} \approx$ 22.5mA. This implies that the laser needs a minimum of 22.5mA current to begin lasing. The optical power output from the L-I curve in figure **9** is P = 13mW when the gain current is 120mA, which is better than the optical power output found by L. Han *et al.* [11], D. Zhou et al. [10], and by D. Zhou et al. [9] at the same gain current. The I_{th} found in this work ($I_{th} \approx$ 22.5mA) is also lower than the I_{th} found by L. Han *et al.* [11] and D. Zhou et al. [10] works who had 25mA and 24mA for threshold currents, respectively.

C. Bragg Section Reflectance

The main purpose of the Bragg section is wavelength tuning. The DBR laser design was to operate in the 1300nm telecommunications window. Therefore, the desired reflectance was in this above-mentioned window. The Bragg section circuit illustrated in figure **4** was simulated using the Bragg section parameters listed in table **2**. The resulting reflectance is shown in figure **10.** From the Reflectance graph, it was observed that the designed Bragg section was capable of performing wavelength selectivity in the 1300nm telecommunications window.

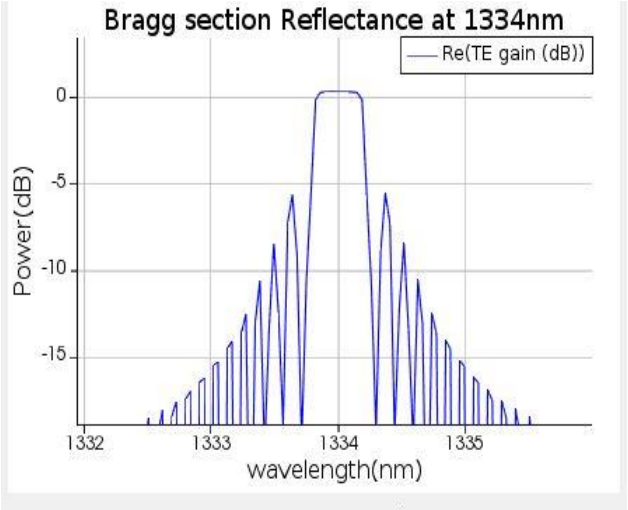

Fig. 10 Bragg section Reflectance over a range of wavelengths in the 1300nm window as designed in Lumerical.

D. Side mode suppression ratio (SMSR)

Below is figure **11**, showing the spectrum of the DBR laser designed in figure **5**. The spectrum is of the transmitted wavelength as tuned by the Waveguide Bragg Grating (WBG_3) circuit.

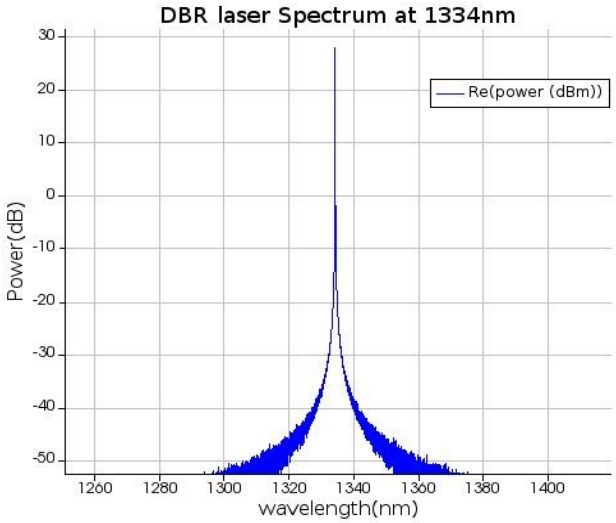

Fig. 11 DBR Laser spectrum

An SMSR of at least 45dB was obtained, which showed much improvement than those SMSR reported in the literature. We therefore report a better SMSR than [10][37][38] who reported SMSRs of 35dB, 30dB and 30dB respectively. Table 3 is a summary and comparison of the results obtained and those found in the literature

Table 3. Results comparison

Ref.	Active Region Material used	Operating wavelength Window	Tuning range	SMSR	Threshold current	Optical Output power at Gain medium current
[12]	Not specified	1500nm	8nm	50 dB	9 mA	0.13 W at 1A
[11]	InGaAsP	1400nm	20nm	30 dB	25 mA	12 mW at 150 mA
[10]	InGaAlAs	1500nm	14.28nm	35 dB	24 mA	10. 3 mW at 100 mA
[37]	III-V-on-silicon	1500nm	12nm	30 dB	55 mA	0.4 mW at 120 mA
[38]	InGaAsP	1800nm	11nm	30 dB	30 mA	6.9 mW at 100 mA
[39]	Not specified	Not specified	17nm	38 dB	Not specified	5.6 mW
[40]	InGaAs/ InGaAsP	1600nm	16nm	34 dB	19 mA	10.3 mW at 100 mA
[41]	InGaAsP	1300nm	15nm	35 dB	13 mA	25 mW at 150 mA
This work	Vanadium doped SiC	1300nm	22nm	45 dB	22.5 mA	13 W at 120 mA

E. Tuning

The current injection tuning mechanism was implemented. The desired wavelength (λ_0 = 1334nm) was set in the Bragg section, and the phase section was used to adjust the cavity to achieve a single-mode operation. In the experiment, the lasing wavelength output was slightly off by a few nanometres (between 0.05nm and 0.1nm) from the desired wavelength, the current from the Direct Current Source labelled DC_4 in figure **5** was adjusted to tune to the required wavelength. If the emitted wavelength was slightly higher than the required wavelength, the current of DC_4 was reduced, which in turn reduced the emitted wavelength through the modulator. And when the emitted wavelength was slightly lower than the desired wavelength, the current was increased in DC_4, which in turn increased the emitted wavelength. Therefore, the phase section was used to get the exact desired wavelength.

IV. CONCLUSION

A three-section tunable laser was designed, simulated, and analyzed using V doped SiC as the active region material. The Material V doped SiC is a new compound that was proposed and used in this work. It is a material that was not in the material database of the Ansys Lumerical design software and hence the reliance on other research works for optical constants data. The active region (Fabry-Perot) was then designed using the calculated optical constants. From literature, it was shown that Vanadium doped silicon carbide radiates in the 1300nm telecommunication window. The calculations indicate that its bandgap energy is 0.93 eV. Based on the relation of Moss, the refractive index was found to be 3.179. The measurements for the length of the active region and the active region thickness were taken from the commonly used active region thickness and active region length and were referenced accordingly. Several iterations were done whilst reducing/increasing the active region thickness and active region width. A comparison with recent works was made, and it was established that the designed laser in this work has better performance than most, as shown in table 5, with a tuning range of over 22nm being observed. A good SMSR of at least 45dB is also obtained. A threshold current of 22.5mA was achieved with an optical output power of 13mW at the gain current of 120mA. The DBR laser has a simple three-section structure which makes its fabrication cheaper. The compound silicon-carbide and the element Vanadium exist freely in nature and have good optical properties making the active region material have low cost in fabrication. Better results can be obtained in the lab when fabricating the actual laser and carrying out the semiconductor doping.

Future works can include the use of V doped SiC in other laser products, such as mid-infrared lasers that can be used for wireless optical communications. In this system of communication, the LEDs are to be implemented with modulators to send light signals to be received by communication devices. The frequency will be in the visible range of the spectrum, and SiC can radiate in that range without doping of metal impurities [14]. This makes it a suitable candidate for the visible light communication systems LEDs in the near future.

V. AUTHORS CONTRIBUTIONS

This research was carried out by Patrick Mumba with the help of two supervisors assigned by Pan African university, institute of basic sciences, technology, and innovation. The gathering of data, calculations, design of the experiment, simulations, and analysis of results was carried out by Patrick Mumba, and the supervision was done by Professor Stephen Musyoki and Doctor Franklin Manene.

VII. ACKNOWLEDGMENTS

The financial support was provided by the Pan African University, institute for basic Sciences, Technology and Innovation, hosted by Jomo Kenyatta University of agriculture and technology in Nairobi, Kenya.

VIII. AVAILABILITY OF DATA

The data used in this work is referenced and available in public domains

IX. CONFLICT OF INTEREST

A Declaration of no conflict of interest is made by the Authors.

X. ADDITIONAL INFORMATION

No additional information for this article

REFERENCES

[1] S. Barrie and D. B. O. Konditi, Evaluation of adjacent channel interference from the land-earth station in motion to 5G radio access network in the Ka-frequency band, Heliyon, 7(6) e07412, DOI: 10.1016/j.heliyon.2021.e07412, 2021.

[2] M. Holmberg, Transport Network Requirements and Architecture for 5G Metro Networks Architecture 2015, Extrem. Cust. Netw., (2018).

[3] S. Tayal, S. K. Goel, and K. Sharma, A Comparative Study of Various Generations in Mobile Technology, Int. J. Eng. Trends Technol., 28(7) (2015) 3, DOI:10.14445/22315381/IJETT-V28P263.

[4] C. V. Dharani and D. B. Terese A, Cross Phase Modulation in multiband Radio- Over-Fiber Systems, Int. J. Eng. Trends Technol., 32(4) (2016) 1 Doi: 10.14445/22315381/it-v32p231,

[5] S. A. Niazi, Integration of Hybrid Passive Optical Networks (PON) with Radio over Fiber (RoF), Intech, Tourism, 1 (2019) 13, Doi:10.5772/intechopen.79299,

[6] M. Bustillos and G. Rinalde, Embedded Tunable Laser Control for WDM Optical Communications Systems, IEEE Lat. Am. Trans., 18(2) (2020) 241–248, DOI:10.1109/TLA.2020.9085276 .

[7] H. Elfaiki, K. Hassan, G.-H. Duan, C. Jany, and S. Malhouitre, Ultra Wide Hybrid III-V On Silicon Tunable Laser, in 2018 European Conference on Optical Communication (ECOC), 1 (2018) 3–5, DOI: 10.1109/ECOC.2018.8535328.

[8] S. Dhoore, G. Roelkens, and G. Morthier, InP-on-Silicon Electronically Tunable Lasers, in 2018 20th International Conference on Transparent Optical Networks (ICTON), (2018)1–4, DOI: 10.1109/ICTON.2018.8473935.

[9] D. Zhou et al., 10 Gb/s Data Transmissions Using a Widely Tunable Directly Modulated InGaAlAs/InGaAsP DBR Laser, IEEE Photonics Technol. Lett., 30(22) (2018) 1. doi: 10.1109/LPT.2018.2872994.

[10] D. Zhou, Y. He, D. Lu, S. Liang, L. Zhao, and W. Wang, 25 Gb/s data transmission using a directly modulate Photonics, 8(3) (2021) 2–6, DOI:10.3390/photonics8030084

[11] L. Han et al., DBR Laser with over 20nm Wavelength Tuning Range, 1135(c) (2016) 3–6, doi: 10.1109/LPT.2016.2518806, .

[12] Y. Zhu, Y. Wu, H. Xu, C. Browning, L. P. Barry, and S. Member, Experimental Demonstration of a WDM-RoF Based Mobile-fronthaul with f-OFDM Signals by Using Directly Modulated 3s-DBR Laser, J. Light. Technol., pp(c) (2019) 1 DOI: 10.1109/JLT.2019.2923245.

[13] S. A. Sobhani et al., Study of electro-absorption effects in 1300nm In(Ga)As/GaAs quantum dot materials, in Physics and Simulation of Optoelectronic Devices XXIV, 9742 (2021) 1. doi:10.1117/12.2213187.

[14] S. Marjani, R. Faez, and H. Marjani, Analysis and Design of Semiconductor Laser with Silicon Carbide Polymers (6H-SiC and 3C-SiC), 5(7) 1–3, doi: ajbas/2011/July-2011/1060-1063.

[15] D. Zhou, S. Liang, L. Zhao, H. Zhu, and W. Wang, High-speed directly modulated widely tunable two-section InGaAlAs DBR lasers, Opt. Express, 25(3) (2017) 2341, doi: 10.1364/OE.25.002341,.

[16] S. Majety, V. A. Norman, L. Li, M. Bell, P. Saha, and M. Radulaski, Quantum photonics in triangular-cross-section nanodevices in silicon carbide OPEN ACCESS Quantum photonics in triangular-cross-section nanodevices in silicon carbide, (2021) 1–3, DOI: 10.1088/2515-7647/abfdca.

[17] N. Tien Son et al., Electron paramagnetic resonance and theoretical studies of Nb in 4H- and 6H-SiC, J. Appl. Phys., 112(8) (2012) 1. doi:10.1063/1.4759362, 2012.

[18] W. F. Koehl et al., "Resonant optical spectroscopy and coherent control of C r4+ spin ensembles in SiC and GaN, Phys. Rev. B, 95(3) (2017) 1-2 . doi: 10.1103/PhysRevB.95.035207.

[19] M. Rejhon, M. Brynza, R. Grill, E. Belas, and J. Kunc, Investigation of deep levels in semi-insulating vanadium-doped 4H-SiC by photocurrent spectroscopy, Phys. Lett. A 405 (2021) 1.DOI: 10.1016/j.physleta.2021.127433, 2021.

[20] F. Fuchs et al., Silicon carbide light-emitting diode as a prospective room temperature source for single photons," Sci. Rep., 3 (2013) 1, Doi: 10.1038/srep01637.

[21] S. Castelletto, Silicon carbide single-photon sources : challenges and prospects Silicon carbide single-photon sources : challenges and prospects, mater. Quantum. technol., 1(2) (2021) 3, Doi: 10.1088/2633-4356/abe04a, 2021.

[22] M. Mahmoodi and L. Ghazanfari, Silicon Carbide: A Biocompatible Semiconductor Used in Advanced Biosensors and BioMEMS/NEMS, Phys. Technol. Silicon Carbide Devices, (2012) 1–3, doi:10.5772/51811.

[23] T. Bosma et al., Identification and tunable optical coherent control of transition-metal spins in silicon carbide, npj Quantum Inf., 4(1) (2018) 1, doi.org/10.1038/s41534-018-0097-8.

[24] G. Wolfowicz, C. P. Anderson, B. Diler, O. G. Poluektov, F. J. Heremans, and D. D. Awschalom, Vanadium spin qubits as telecom quantum emitters in silicon carbide, (2020) 2–10, doi:10.1126/sciadv.aaz1192.

[25] L. Spindlberger et al., Optical Properties of Vanadium in 4 H Silicon Carbide for Quantum Technology, Phys. Rev. Appl., 10(1) (2019) 1–3, https://doi.org/10.1103/PhysRevApplied.12.014.

[26] N. J. Kramer et al., Extrinsic Absorption Pathways in Vanadium-Doped SiC Measured Using a Total Internal Reflection Geometry, Phys. Status Solidi Appl. Mater. Sci., 217(20) (2020) 1. doi: 10.1002/pssa.202000315, Oct.

[27] R. T. Sutter, T. J. Fellers, and M. W. Davidson, Laser Cavity Resonance Modes and Gain Bandwidth - Java Tutorial | Olympus LS. [Online]. Available: https://www.olympus-lifescience.com/en/microscope-resource/primer/java/lasers/gainbandwidth/. [Accessed: 05-Aug-2021].

[28] B. Van Zeghbroeck, LASER DIODES, in Principles of Semiconductor Devices, 82(1–2) (2004) 223, doi: 10.1016/j.solmat.2004.01.028.

[29] Z. Ma et al., A zero-cross detection algorithm for cavity-length interrogation of fibre-optic fabry–Perot sensors, Sensors (Switzerland), 19(18) (2019) 11, doi: 10.3390/s19183868 .

[30] DBR laser using travelling wave laser model (TWLM) – Lumerical Support. [Online]. Available: https://support.lumerical.com/hc/en-us/articles/360042326114-DBR-laser-using-travelling-wave-laser-model-TWLM-. [Accessed: 21-Jun-2021].

[31] Laser TW (TWLM) - INTERCONNECT Element – Lumerical Support. [Online]. Available: https://support.lumerical.com/hc/en-us/articles/360036108274-Laser-TW-TWLM-. [Accessed: 24-Jul-2021].

[32] Â. R. Costa, W. Ulrich, and J. G. Correia, Lattice location of impurities in Silicon Carbide, PHD thesis Phys. Univ. LISBOA Inst. Super. TÉCNICO, 20 (2018).

[33] N. M. Ravindra, P. Ganapathy, and J. Choi, Energy gap-refractive index relations in semiconductors - An overview, Infrared Phys. Technol., 50(1) (2007) 21-22, DOI:10.1016/j.infrared.2006.04.001.

[34] M. De Laurentis and A. Irace, Optical Measurement Techniques of Recombination Lifetime Based on the Free Carriers Absorption Effect, J. Solid State Phys., (2014) 2, doi: 10.1155/2014/291469.

[35] G. P. Agrawal, Optical transmitters, in Fiber-Optic Communications Systems, Third Edition., 3rd ed., john Wiley and sons, 6 (2002) 77–78.

[36] Y. Zhao et al., Spontaneous emission factor for superluminescent semiconductor diodes Spontaneous emission factor for

superluminescent semiconductor diodes, J. Appl. Phys., 3945(1999) 5 (3948), doi: 10.1063/1.370294.

[37] S. Dhoore, G. Roelkens, and G. Morthier, III-V-on-silicon three-section DBR laser with over 12 nm continuous tuning range, Opt. Lett., 42(6) (2017) 1, doi: 10.1364/ol.42.001121,

[38] H. Yu, J. Pan, X. Zhou, H. Wang, L. Xie, and W. Wang, A widely tunable three-section dbr lasers for multi-species gas detection, Appl. Sci., 11(6) (2021) 1, DOI:10.3390/app11062618.

[39] H. Conradi et al.,Tunable DBR Laser with Integrated Optical Isolator, in Optical Fiber Communication Conference (OFC) (2021)1.

[40] H. Yu et al., A 1.6-μm widely tunable distributed Bragg reflector laser diode based on InGaAs/InGaAsP quantum-wells material, Opt. Commun., 497 (2021) 1, doi.org/10.1016/j.optcom.2021.127201 .

[41] O. K. KWON, C. W. LEE, S. H. OH, and K. S. KIM, 16-channel tunable and 25-Gb / s EAM-integrated DBR-LD for WDM-based mobile front-haul networks, Opt. Express, 29(2) (2021) 1 .doi.org/10.1364/OE.414989.